

A model system for two-dimensional and three-dimensional photonic crystals: macroporous silicon

J Schilling¹, R B Wehrspohn¹, A Birner^{1,2}, F Müller¹,
R Hillebrand¹, U Gösele¹, S W Leonard³, J P Mondia³,
F Genereux³, H M van Driel³, P Kramper⁴, V Sandoghdar⁴
and K Busch⁵

¹ Max Planck Institut für Mikrostrukturphysik, Weinberg 2, D-06120 Halle, Germany

² Infineon Technologies, Memory Products, D-01099 Dresden, Germany

³ Department of Physics, University of Toronto, 60 St George Street, Toronto, Ontario, Canada M5S 1A7

⁴ Universität Konstanz, Fachbereich Physik, Fach M696, D-78457 Konstanz, Germany

⁵ Institut für Theorie der Kondensierten Materie, Universität Karlsruhe, D-76128 Karlsruhe, Germany

Received 11 July 2001

Published 26 October 2001

Online at stacks.iop.org/JOptA/3/S121

Abstract

A review of the optical properties of two-dimensional and three-dimensional photonic crystals based on macroporous silicon is given. As macroporous silicon provides structures with aspect ratios exceeding 100, it can be considered to be an ideal two-dimensional photonic crystal. Most of the features of the photonic dispersion relation have been experimentally determined and were compared to theoretical calculations. This includes transmission and reflection of finite and bulk photonic crystals and their variation with the pore radius to determine the gap map. All measurements have been carried out for both polarizations separately since they decouple in two-dimensional photonic crystals. Moreover, by inhibiting the growth of selected pores, point and line defects were realized and the corresponding high- Q microcavity resonances as well as waveguiding properties were studied via transmission. The tunability of the bandgap was demonstrated by changing the refractive index inside the pores caused by an infiltrated liquid crystal undergoing a temperature-induced phase transition. Finally different realizations of three-dimensional photonic crystals using macroporous silicon are discussed. In all cases an excellent agreement between experimental results and theory is observed.

Keywords: Photonic crystal, two-dimensional, three-dimensional, macropores, macroporous silicon, birefringence, defects, tunability

From the beginning of research on photonic crystals, a major area of investigation concerned two-dimensional photonic crystals [1]. This was mainly caused by experimental reasons as the fabrication of three-dimensional photonic crystals appeared to be more difficult and cumbersome than that of two-dimensional photonic crystals. Additionally the calculation of bandstructures for two-dimensional photonic crystals is less time consuming and a lot of interesting phenomena (e.g. light

localization; at least in a plane) can already be studied in two-dimensional photonic crystals.

However, an ideal two-dimensional photonic crystal consists of a periodic array of infinitely long pores or rods so that the fabrication of a structure which approximates this theoretical model has to exhibit very high aspect ratios (ratio between pore/rod length to pore/rod diameter). Using conventional dry etching techniques only structures with aspect

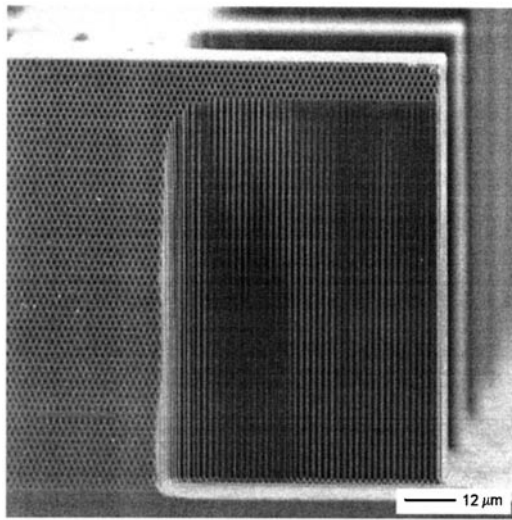


Figure 1. SEM image of a two-dimensional triangular lattice of macropores in silicon with a lattice constant of $1.5 \mu\text{m}$. As the pore depth amounts to $100 \mu\text{m}$ the aspect ratio is ~ 100 . The bevelled etch in front reveals the high uniformity of the structure from the top down to the pore tips.

ratios up to 10–20 are possible. To avoid scattering of light out of the plane of periodicity and to reduce the corresponding loss the so-called slab structures were developed and thoroughly investigated [2, 3]. In such low-aspect structures, one relies on guiding of light in the third dimension and, consequently, deals with a full three-dimensional problem. On the other hand Lehmann and Grüning [4, 5] as well as Lau and Parker [6] proposed macroporous silicon as a model system for two-dimensional photonic crystals. This system consists of a periodic array of air pores in silicon. The pores are etched in hydrofluoric acid applying a photo-electrochemical dissolution process [7, 8]. Using lithographic prestructuring the nucleation spots of the pores can be defined at the surface of the n-type silicon wafer. This also allows the pore pattern and its lattice constant to be controlled over the range from $8 \mu\text{m}$ down to $0.5 \mu\text{m}$. During the etching process the back of the wafer must be illuminated to create electronic holes in the silicon which are consumed during the etching process. Due to electrochemical passivation of the pore walls very high aspect ratios of 100–500 are obtained. As the fundamental bandgap appears in general for wavelengths which are approximately twice the lattice constant, the pores are 50–250 times longer than the wavelengths of the corresponding two-dimensional fundamental bandgap. Therefore, macroporous silicon represents an excellent system to study ideal two-dimensional photonic crystal properties.

In figure 1(a) a structure with a triangular two-dimensional pore lattice with a lattice constant of $1.5 \mu\text{m}$ is shown. The pore depth is $100 \mu\text{m}$ and the bevelled edge reveals the high uniformity of the pores down to the pore tips.

In the next paragraphs optical experiments performed with such structures are presented and compared with calculations assuming a two-dimensional array of infinitely long macropores. The lattice type, lattice constant and the pore depth of the investigated structures have the same values as the sample shown in figure 1 while the diameter of the pores varies in order to meet the experimental requirements.

1. Two-dimensional photonic crystals based on macroporous silicon

The dispersion relation for light propagation inside a photonic crystal is calculated using the plane-wave method. Due to the two-dimensional periodicity and the uniformity along the third dimension the light propagating in a two-dimensional photonic crystal splits into E-polarized (E-field parallel to the pore axis) and H-polarized (H-field parallel to the pore-axis) waves. The bandstructures for these polarizations differ from each other and so do the bandgaps in width and spectral position. This originates in the different field distributions: typically, the electric field of the H-polarized waves is located in the veins of the structures whereas the electric field of the E-polarized waves concentrates in the connection points of the veins. Figure 2(a) shows an example of a bandstructure for our system calculated for wavevectors in the first Brillouin zone along the path Γ -M-K- Γ . The assumed porosity or air filling factor is $p = 0.73$ which corresponds to $r/a = 0.45$ ($r =$ pore radius, $a =$ lattice constant) and the refractive index of silicon in the infrared (IR) is 3.4. For a triangular array of pores, a refractive-index contrast exceeding 2.7 [9] and suitable r/a ratios the bandgaps for E- and H-polarization overlap and a complete two-dimensional photonic bandgap exists. As the refractive-index contrast for air pores in silicon amounts to $\epsilon_{\text{Si}}/\epsilon_{\text{Air}} = 3.4$ in the IR, these requirements are fulfilled in our system. The bandstructure shown in figure 2 thus exhibits such a complete bandgap indicated by a grey bar.

In addition to the bandstructure, the density of photonic states (DOS) is computed as well and presented in figure 2(b). In the spectral region of the complete photonic bandgap the DOS is zero, such that propagation of light in the plane of periodicity with these frequencies is completely forbidden in the photonic crystal.

To verify these theoretical calculations, transmission measurements through bars of the macroporous silicon photonic crystals along Γ -M and Γ -K directions were carried out. For this purpose bars containing 13 pore rows were cut out using a second lithographic step. The measurements were performed using a Fourier transform infrared spectrometer (FTIR) in the spectral range between 700 and 7000 cm^{-1} (14.3 and $1.43 \mu\text{m}$). Figure 3 shows the measured spectra for both directions and both polarizations. They are compared to transmission calculations using the method developed by Sakoda [10]. The spectral positions of regions with vanishing transmission correspond well to the calculated spectrum. For the measurements along the Γ -M direction they can be attributed to the bandgaps already discussed in figure 2 for H-polarized and E-polarized light. However, the vanishing transmission in the range of 2200 – 3500 cm^{-1} for propagation along the Γ -K direction of E-polarized light cannot entirely be explained through a stopband. A comparison with the bandstructure of figure 2 predicts a photonic band which covers part of this spectral region. However, as was pointed out earlier [11, 12] bands in which the experimentally incident plane wave cannot couple also lead to zero transmission. These bands correspond to Bloch modes whose field distributions are antisymmetric with respect to the plane spanned by the pore axis and the direction of incidence. Consequently, although modes do exist in the photonic crystal they need not to be

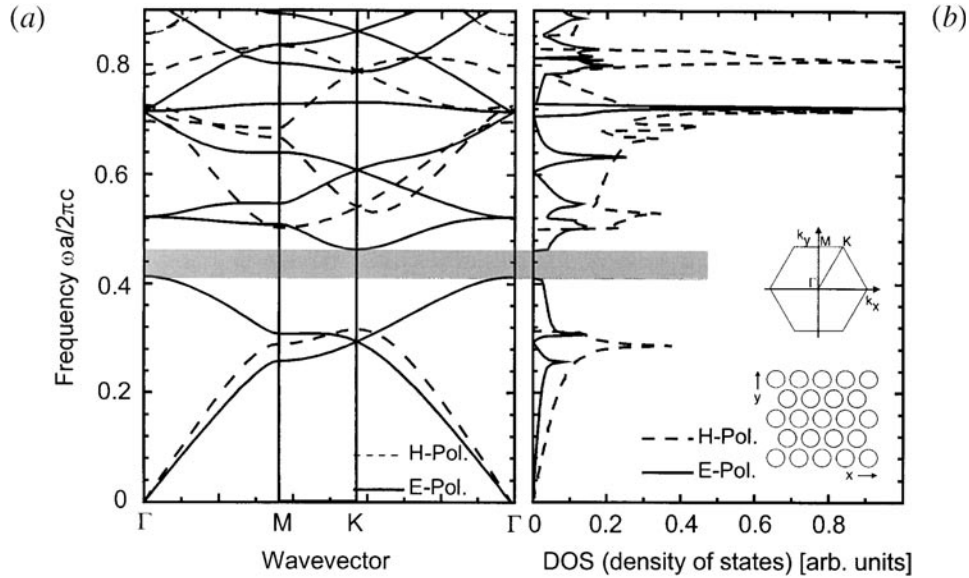


Figure 2. (a) Two-dimensional bandstructure of a triangular macroporous silicon photonic crystal ($r/a = 0.45$). (b) DOS, inset: two-dimensional hexagonal Brillouin zone and appropriate oriented triangular pore lattice in real space. The grey bar indicates the two-dimensional complete bandgap. In this spectral range neither H- nor E-polarized photonic states exist (DOS = 0).

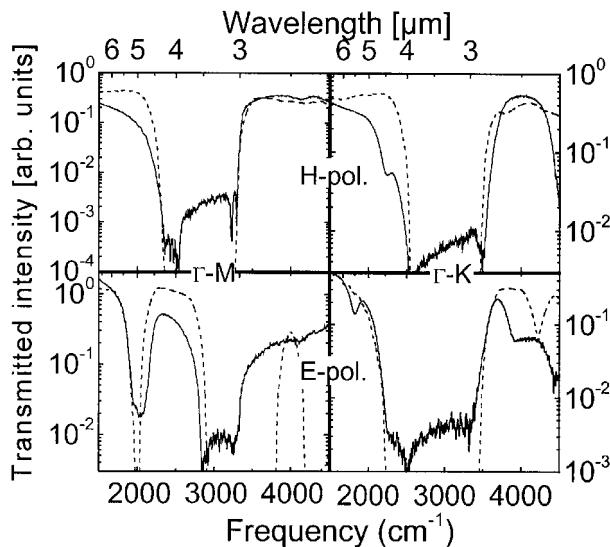


Figure 3. Transmission measurements (solid curve) and calculation (dashed curve) for penetration of a two-dimensional macroporous silicon photonic crystal bar containing 13 pore rows. Transmission for both polarizations (H- and E-polarization) along both high-symmetry directions, Γ -M and Γ -K, are shown.

visible in transmission. Therefore, care has to be taken when directly comparing reflection or transmission measurements with bandstructures: although a bandgap leads always to total reflection/zero transmission, a spectral region exhibiting total reflection/zero transmission does not necessarily coincide with a bandgap. A direct comparison of experiment and theory is therefore rather based on reflection/transmission calculations than on bandstructure calculations alone. In addition to the applied Sakoda method, mainly transfer-matrix and finite difference time domain (FDTD) methods can be used for the calculation of reflection and transmission.

The complete bandgap derived from the bandstructure calculations comprises the interval between 2900 and 3300 cm^{-1} (3.44 and 3.03 μm). It clearly overlaps with all spectral regions with vanishing transmission.

The optimum bandgap cannot be understood by Bragg scattering only. For scatterers whose spatial dimensions are comparable to the wavelength, additional scattering resonances (known as Mie resonances for spherical particles) appear. They depend on the size and shape of the scatterers. Consequently, apart from symmetry, lattice constant and refractive index, the radius of the pores (r/a -ratio) has an influence on the existence, position and the width of the photonic bandgaps. A graphic representation of the relationship between gap frequencies and filling ratio is known as a gap map, which for our structure, has been calculated before [1]. To verify this gap map experimentally, transmission measurements for 17 different samples spanning a wide range of r/a -ratios were carried out. The bandedges were determined from these measurements and are compared with the theoretical predictions in figure 4. The overall correspondence is very good. For lower r/a -ratios only a bandgap for the H-polarization exists. A complete bandgap only appears for $r/a > 0.4$ as then an E-bandgap appears which overlaps with the H-bandgap. With increasing r/a -ratios the E-bandgap widens while the H-bandgap shrinks for very high filling ratios. A maximum complete bandgap of $\Delta\omega/\omega = 16\%$ for $r/a = 0.48$ can be deduced. This relatively large complete bandgap is a consequence of the strong refractive-index contrast between the silicon (pore walls) and air (inside the pores) as well as the synergetic interplay of Mie resonance and Bragg scattering resonance.

Strictly speaking, the bandstructure calculations can only be performed assuming an infinitely extended photonic crystal. Therefore also the bandgap (zero DOS) causing perfect total reflection only appears for infinite bulk photonic crystals. For a very thin slab of the photonic crystal the incident

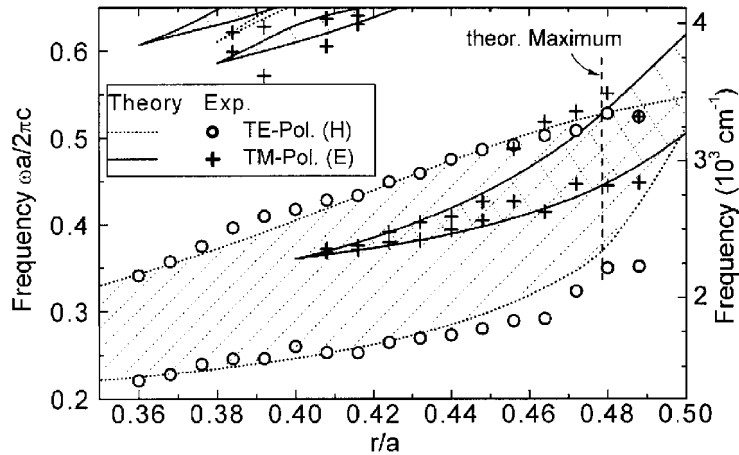


Figure 4. Position of the bandgaps for H-polarized light (dotted curve) and E-polarized light (solid curve) for a two-dimensional triangular macroporous silicon photonic crystal depending on the r/a -ratio (gap map). A complete bandgap appears as an overlap of the gaps for both polarizations and attains its maximum size with a r/a -ratio of 0.48.

light of a frequency within the bulk bandgap is no longer *totally* reflected. A certain amount can penetrate the thin photonic crystal. To investigate this effect four samples containing one, two, three and four crystal rows with a r/a -ratio of 0.453 were fabricated (figure 5(a)). Transmission measurements for H-polarized light of different wavelengths along Γ -K were performed (see figure 2) [13]. A tunable laser set-up was used which covered the spectral range between $3 < \lambda < 5 \mu\text{m}$ corresponding to the range of the H-bandgap ($3.1 < \lambda < 5.5 \mu\text{m}$) of the corresponding bulk photonic crystal. The experimental results were compared with transmission calculations applying the already mentioned Sakoda method with 4000 plane waves and revealed a very good agreement (figure 5(b)). Plotting the transmittance versus the penetrated crystal thickness (figure 5(c)) an exponential decay is observed. This corresponds to the expectation that for frequencies within the bandgap the light penetrating into the bulk photonic crystal is exponentially damped. The slope of the line in the logarithmic plot corresponds to a decay constant of 10 dB per crystal row for light with a wavelength near the centre of the bandgap. Even for a bar containing only one pore row the bandgap is already perceptible. This originates in the strong scattering of the single pores due to the large refractive-index contrast between air pores and silicon walls.

In the initial investigations into photonic crystals mostly photonic bandgap properties were studied. However, over the last few years attention has also been drawn to other spectral regions of the dispersion relation that exhibit remarkable properties.

For instance, we recently investigated the birefringence of a two-dimensional macroporous silicon photonic crystal in the spectral region below the first bandgap. From theoretical investigations [14, 15] it was expected that a triangular two-dimensional photonic crystal shows uniaxial properties for $\omega \rightarrow 0$. The optical axis coincides in this case with the pore/rod axis. For light propagating in this direction the effective refractive index is independent of the polarization direction (birefringence = 0). However for light propagating in the plane of periodicity the two-dimensional bandstructure reveals different slopes of the E- and H-polarized bands due to different mode distributions in the silicon matrix. This

corresponds to different effective refractive indices for these two different polarizations and leads to birefringent behaviour of light propagation perpendicular to the pore axis. We investigated this effect experimentally in transmission using an FTIR spectrometer. The sample consisted of a macroporous silicon crystal with a lattice constant $a = 1.5 \mu\text{m}$ and r/a -ratio of 0.429. The transmission along the Γ -M direction through a bar of $235 \mu\text{m}$ width containing 181 pore rows was measured [16]. In front of the sample a polarizer was placed and aligned with an angle of 45° relative to the pore axis. This defined a certain polarization state of the light incident on the photonic crystal and assured that the radiation consisted of H- and E-polarized components of comparable strengths. After penetration through the sample the beam passes through a second polarizer which is aligned parallel or perpendicular to the first polarizer, respectively. The measured transmission for parallel and crossed polarizers is shown in figure 6. A periodic variation of the transmitted intensity is observed for both polarizer set-ups. The maxima of the parallel polarizer orientation corresponds to the minima of the crossed orientation. This can be explained considering the phase difference which builds up between E- and H-polarized light after penetration through the photonic crystal. This phase difference is given by $\Delta\phi = 2\pi\Delta n_{\text{eff}}df/c$ (Δn_{eff} difference of effective refractive indices, d thickness of penetrated photonic crystal, f light frequency). For parallel orientations of the polarizers a maximum occurs for $\Delta\phi = 2m\pi$ while a minimum appears for $\Delta\phi = (2m+1)\pi$. For the crossed polarizers the opposite is true. The light frequency and the order of the maxima and minima are determined from the transmission curve and with this the birefringence Δn_{eff} can be calculated. It is frequency dependent (figure 7). However, over the entire investigated spectral range its value exceeds 0.3 and attains its maximum at the upper limit of the investigated range (at the lower bandedge of the first E-gap). The largest birefringence measured amounts to 0.366 at a frequency $f = 0.209c/a$. With this it is by a factor of 43 larger than the birefringence of quartz.

The uniaxial behaviour of the triangular two-dimensional photonic crystal in the limit $\omega \rightarrow 0$ corresponds to the well

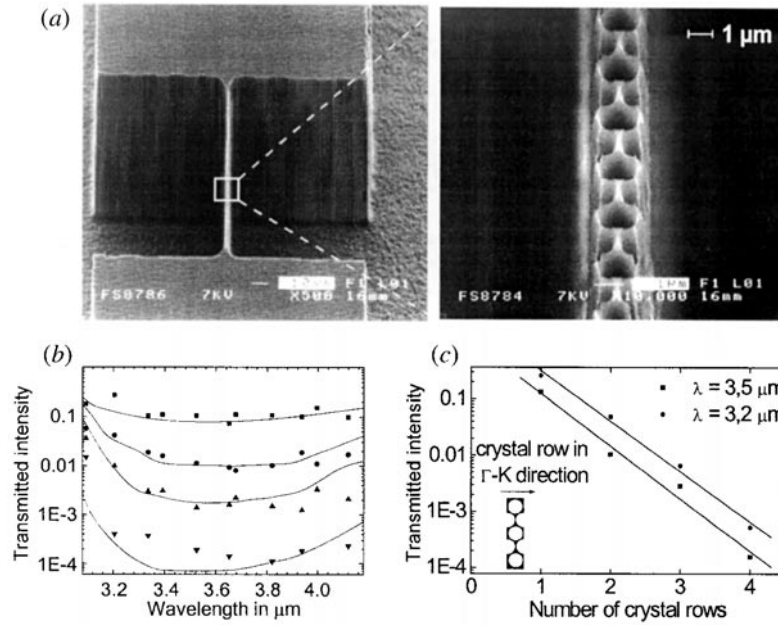


Figure 5. (a) SEM image of the macroporous silicon bars with varying thickness. The inset shows an enlarged view of the centre square. (b) Measured and calculated transmission for wavelengths within the H-bandgap. Solid curves, calculations for transmission through one, two, three and four crystal rows. Points: measurements for 0.89 ± 0.04 (■), 1.8 ± 0.1 (●), 2.9 ± 0.1 (▲) and 4.2 ± 0.2 (▼) crystal rows. (c) Measured transmission as a function of slab thickness for two wavelengths within the bandgap.

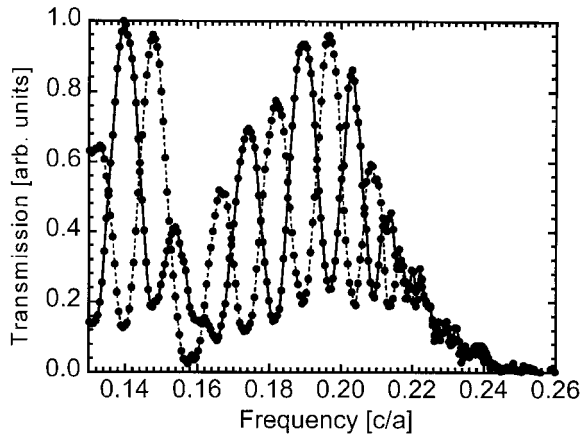


Figure 6. Effect of birefringence: measured transmission in the spectral range below the first bandgap (long wavelength regime). Spectra were recorded for parallel (solid curves) and crossed (dashed curves) orientations of the two polarizers which were placed in front and behind the sample, respectively. The periodic maxima and minima in the transmission spectrum appear due to the phase difference between E- and H-polarized waves accumulating during penetration of the sample.

known uniaxial birefringence of hexagonal atomic crystals in the visible region. In atomic crystals the scatterers (atoms) have distances in the region of Å and therefore Bragg diffraction occurs for wavelengths in the x-ray region. For these classic atomic crystals the visible region of the spectrum corresponds to the long wavelength limit $\omega \rightarrow 0$. In our case, where the lattice constant is of the order of $1 \mu\text{m}$, Bragg diffraction occurs in the near and mid IR (causing the bandgaps) while the limit $\omega \rightarrow 0$ comprises the long wavelength regions of the mid and far IR.

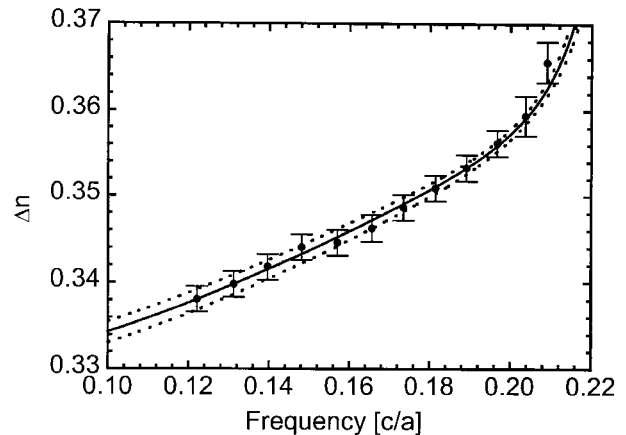


Figure 7. Spectral dependence of birefringence (Δn). Measurements (data points) and calculations (curves). The dashed curves represent the calculated dependence for the upper and lower bounds of the measured value of r/a (0.429 ± 0.002). The largest measured birefringence ($\Delta n = 0.365$) appears near the upper limit of the investigated spectral range close to the bandedge for E-polarization.

In the described experiment only the birefringence along one propagation direction in the plane of periodicity was investigated. For the case of a uniaxial crystal this is sufficient, as the birefringence is constant for all propagation directions perpendicular to the optical axis. However, for increasing light frequencies which approach the first bandgap this is no longer true. In this case the value of the birefringence depends on the direction of propagation in the Γ -M-K plane and the optical properties of the crystal can no longer be described by the terms ‘uniaxial’ or ‘biaxial’ used in classic crystal optics [17].

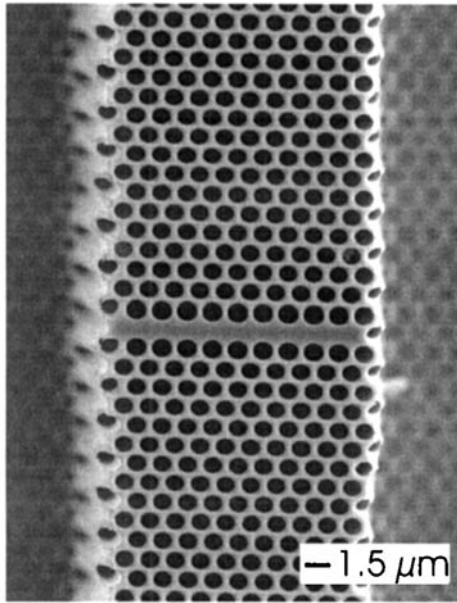


Figure 8. SEM image of a two-dimensional macroporous silicon bar containing a line defect introduced by skipping a line of pore nucleation spots defined by lithography.

2. Defects in two-dimensional macroporous silicon photonic crystals

Since the beginning of the study of photonic crystals special attention was paid to intentional incorporated defects in these crystals. Point or line defects can be introduced into macroporous two-dimensional silicon photonic crystals by omitting the growth of a single pore or a line of pores. This can be achieved by designing a suitable mask for the lithography (the pattern defining process). To demonstrate waveguiding through a linear defect we incorporated a $27\ \mu\text{m}$ line defect along the Γ -K direction into a triangular two-dimensional photonic crystal with a r/a ratio of 0.43 ($r = 0.64\ \mu\text{m}$) [18]. However, due to the photo-electrochemical fabrication process the diameter of the pores in the adjacent rows to the waveguide is increased. Figure 8 shows a picture of a similar structure. The transmission through the line defect was measured with a pulsed laser source having a bandwidth of 200 nm and tunable over the whole width of the H-stopband in the Γ -K direction ($3.1 < \lambda < 5.5\ \mu\text{m}$). The measured spectrum (figure 9) exhibits pronounced Fabry–Perot resonances over a large spectral range which are caused by multiple reflections at the waveguide facets. Comparing the spectrum with a FDTD-transmission calculation reveals very good agreement and the comparable finesse of the measured and calculated resonances indicate small losses in the sample. A bandstructure calculation for H-polarization along Γ -K including waveguide modes is depicted in figure 10. The grey-shaded regions represent all possible modes inside the perfect crystal areas adjacent to the line defect. Defect modes bound to the line defect, therefore, occur only in the range $0.27 < f < 0.46$. They split into even and odd modes with respect to the mirror plane which is spanned by the waveguide direction and the direction of the pore axis. As the incoming wave can be approximated by a plane wave, the incident radiation can only couple to the even modes of the waveguide. The odd modes do

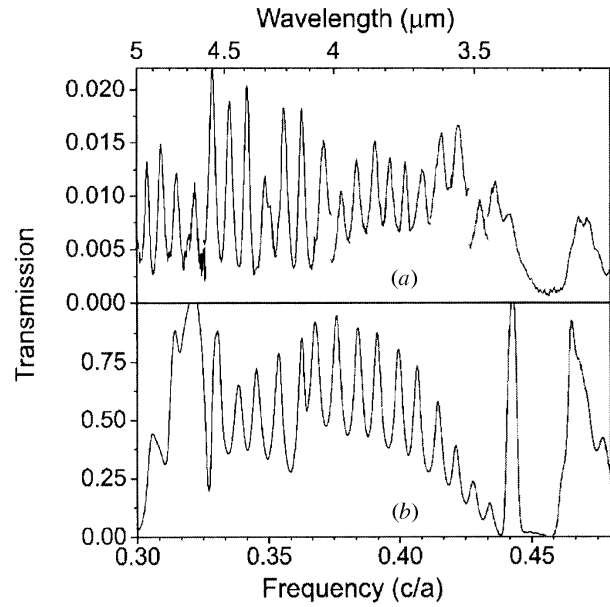


Figure 9. (a) Measured and (b) calculated H-polarized transmission spectrum of a $27\ \mu\text{m}$ -long waveguide directed along Γ -K covering the spectral range of the H-bandgap of the surrounding perfect photonic crystal. Only the *even* waveguide modes contribute to the transmission as the incoming plane wave cannot be coupled to the *odd* waveguide modes. The small stopgap at a frequency of $0.45\ c/a$ is caused by the anticrossing of two even waveguide modes.

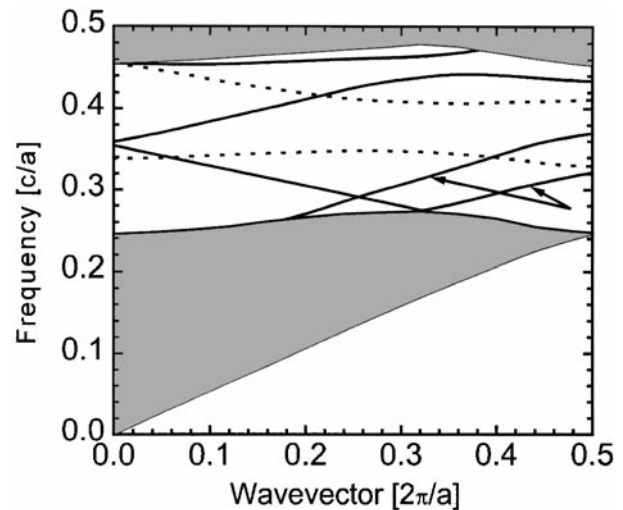


Figure 10. Computed H-polarized bandstructure of the waveguide oriented along Γ -K. Solid and dotted curves correspond to even and odd modes, respectively. The two bands which are labelled with arrows appear due to the overetched pores on either side of the waveguide. The shaded areas correspond to the modes available in the adjacent perfect crystal regions.

not contribute to the transmission through the waveguide and, therefore, in this experiment transmission is solely connected with the even modes. The small stopband between the even modes around a frequency of 0.45 is reproduced as a region of vanishing transmission in figure 9 due to anticrossing of the waveguide modes [19]. Furthermore, from the bandstructure it can be concluded that for $0.37 < f < 0.41\ c/a$ only a single even mode exists. Its bandwidth amounts to 10%.

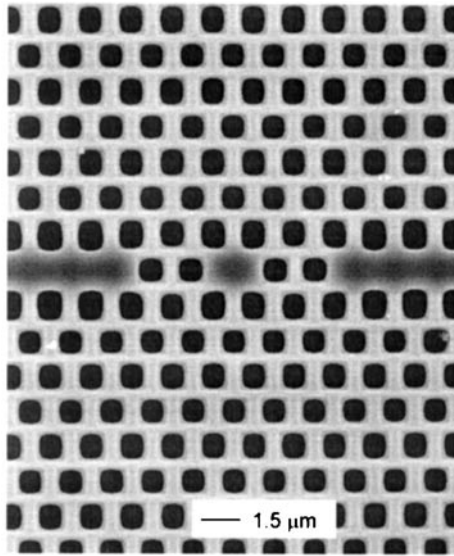


Figure 11. Top view of the photonic crystal region containing the waveguide–microresonator–waveguide structure. The r/a -ratio of the pores amounts to 0.433. The waveguides on the left and right serve to couple the light into the point defect (microresonator).

In addition to line defects point defects consisting of just one missing pore are also of special interest. Such a micro resonator-type defect also causes photonic states whose spectral positions lie in the range of the bandgap of the surrounding perfect photonic crystal. The lightfields belonging to these defect states are therefore confined to the very small volume of the point defect resulting in very high energy densities inside the defect volume. As the point defect can be considered as a microcavity surrounded by perfect reflecting walls, resonance peaks with very high Q -values are expected in the transmission spectra. To study this experimentally we fabricated a sample including a point defect which was placed between two line defects serving as waveguides for coupling light in and out [20]. Figure 11 shows a SEM image of the described sample with $r/a = 0.433$. Measuring transmission through this waveguide–microresonator–waveguide structure demands an optical source with a very narrow linewidth. Therefore, a continuous wave optical parametric oscillator (OPO) has been used which is tunable between 3.6 and 4 μm and delivers a laser beam of 100 kHz linewidth. For spatially resolved detection an uncoated tapered fluoride glass fibre mounted to a scanning nearfield optical microscope-head was applied and positioned precisely to the exit facet of the outcoupling photonic crystal waveguide. In the transmission spectrum two-point defect resonances at 3.616 and 3.843 μm could be observed (figure 12). Their spectral positions are in excellent agreement with the calculated values of 3.625 and 3.834 μm predicted by FDTD calculations taking into account the slightly widened pores surrounding the point defect. The measured point defect resonances exhibited Q values of 640 and 190, respectively. The differences to the theoretical predicted values of 1700, 750 could be caused by very small pore diameter variations (of the order of 1%) with the depth. A slight variation of the resonance frequency with pore depth and a scattering of light out of the plane of periodicity can be the

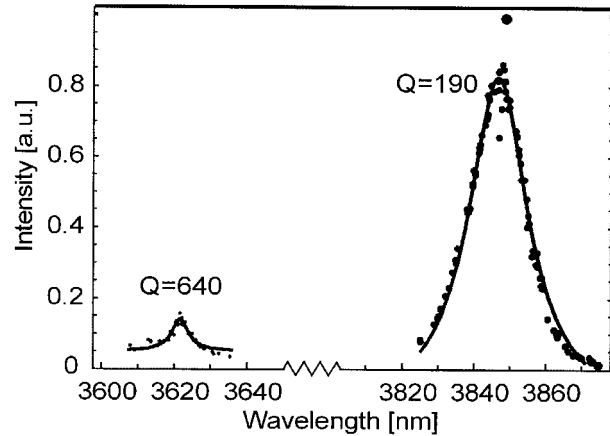


Figure 12. Measured monopole ($Q = 640$) and decapole resonances ($Q = 190$) of the point defect at wavelengths of 3.616 and 3.843 μm .

consequences leading to a broadened averaged resonance peak. However, the reported high Q -values of this two-dimensional microresonator might already be sufficient for studying the modification of radiation properties of an emitter placed in such a point defect. Microcavities with even higher Q -values might be possible by increasing the number of pores to three or four which separate the point defect from the waveguides.

3. Technologically relevant structures

In the preceding paragraphs experiments were reported which demonstrate the properties of macroporous silicon for two-dimensional photonic crystals with bandgaps in the mid IR. Their high accuracy makes them a perfect model system to explore the concept of photonic crystals in the IR region. In addition to their physically interesting properties photonic crystals bear considerable potential for optical telecommunications (for instance, application of line defects for routing of light beams). For these applications photonic crystal waveguides have to work in a wavelength range between 1.3 and 1.5 μm so that they are compatible with the existing glass-fibre network. This fact requires photonic crystals with bandgaps in the corresponding spectral range. As is known from Maxwell's equations the spectral position of the bandgap scales linearly with the lattice constant of the photonic crystals. Therefore, structures with sub-micrometer dimensions are necessary. Although they should not show a novel physical behaviour, their fabrication is still an experimental challenge. We fabricated a triangular lattice with a pitch $a = 0.5 \mu\text{m}$ and a r/a -ratio of 0.425. To check the spectral position of the first-order bandgap, reflection measurements were performed using an IR microscope connected to a FTIR spectrometer. The reflection for H- and E-polarized light incident in the Γ -M direction was measured separately. A gold mirror was used as a reference. Figure 13 shows a comparison of the measured reflection spectra with the bandstructure and with reflection calculations using a programme based on a transfer-matrix approach [21]⁶. The grey-shaded spectral ranges represent the

⁶ The program 'Translight' can be downloaded from <http://www.elec.gla.ac.uk/~areynolds/software.html>. It is based on the paper by Bell *et al* [21].

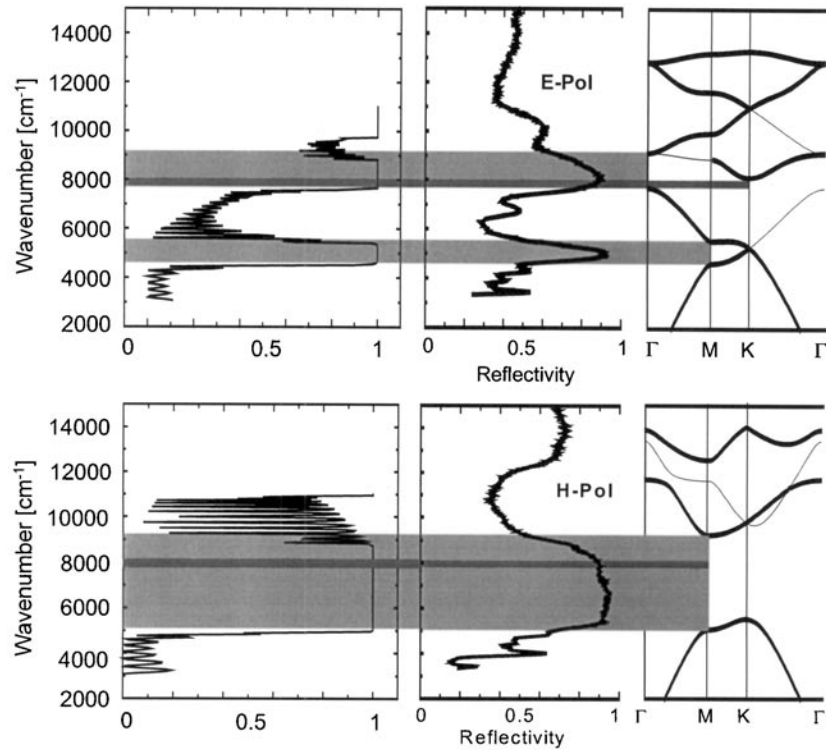


Figure 13. Reflectivity along Γ -M for a two-dimensional triangular macroporous silicon photonic crystal with a lattice constant of $0.5 \mu\text{m}$ for E-polarization (upper part) and H-polarization (lower part). Left, calculated reflectivity assuming a finite photonic crystal containing eight pores rows. The periodic Fabry–Perot resonances are caused by multiple reflections at the facets of the assumed thin bar. Middle, measured reflectivity of a semi-infinite photonic crystal. No resonances appear, as the second facet lies at infinity. Right, comparison with bandstructure. Thick bands contribute to transmission while for the thin bands the incident plane waves cannot couple. In addition to the bandgaps they also cause total reflection (grey-shaded regions). The dark-shaded range shows the complete bandgap around 8000 cm^{-1} ($1.25 \mu\text{m}$).

theoretically expected regions of high reflectivity stemming from the bandgaps. They correspond very well to the experimental results. The thick printed bands are transmission bands while the thin printed bands are bands in which a plane wave cannot couple into the photonic crystal slab. The reflection calculations were carried out assuming a finite bar of the photonic crystal containing eight layers. This finite thickness causes the Fabry–Perot interferences in the spectrum by multiple reflections at the front and back surface of the bar. However, in the experiment we investigated a semi-infinite photonic crystal. In this case the Fabry–Perot resonances are absent. Apart from this difference the calculated reflection curves agree very well with the measured ones and the spectral ranges of very high reflectivity caused by the bandgaps (ideal total reflection) coincide. Although the reflected light contained contributions from beams with an incidence angle of up to 30° (due to the focussing conditions of the microscope) this off-normal incidence has only a negligible effect. The incident light is bent by refraction towards the normal propagating with a much smaller angular deviation inside the photonic crystal. Additionally, the width and position of this first-order bandgap is not very sensitive for small angular deviations [22]. This is the reason why good agreement with the bandstructure along Γ -M and the calculation can be observed. From the calculated bandstructure a complete bandgap in the range 1.22 – $1.3 \mu\text{m}$ can be derived.

Together with the results of Rowson *et al* [23] who showed bandgaps at $1.5 \mu\text{m}$ this experiment proves that

macroporous silicon structures can be fabricated and used as two-dimensional photonic crystals for the technologically interesting telecommunication wavelengths between 1.3 and $1.5 \mu\text{m}$.

As was pointed out earlier the attenuation for light frequencies within the bandgap amounts to 10 dB per pore row. As Maxwell’s equations scale with the structure size this relative property also remains unchanged for the downscaled structure. This enables a close packing of waveguides, as the separation of six to eight pore rows should be sufficient to avoid any cross-talk between neighbouring waveguides.

4. Tunability of photonic bandgaps

Small deviations of the fabricated experimental structures from the designed ones have a serious influence on their optical properties. In particular, the design of a microresonator (point defect) with a well defined resonance frequency in the near IR only allows fabrication tolerances in the sub-nanometre regime, a demand which currently cannot be fulfilled reproducibly. Additionally, for many applications, optical switches for example, one would like to shift the bandgap during operation. Therefore, tuning the optical properties during operation is a major point of interest.

One way to achieve this is to change the refractive index of at least one material inside the photonic crystal. This can be obtained by controlling the orientation of the optical anisotropy of one material incorporated in the photonic crystal [24].

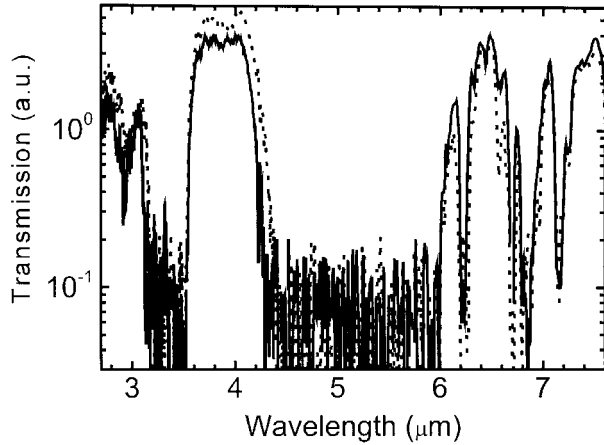


Figure 14. Shift in a bandedge caused by the thermally induced reorientation of an infiltrated liquid crystal: H-polarized transmission along Γ -K after infiltration of the liquid crystal E7. Solid curve, liquid crystal in its nematic phase (35°C); dotted curve, liquid crystal in its isotropic phase (62°C).

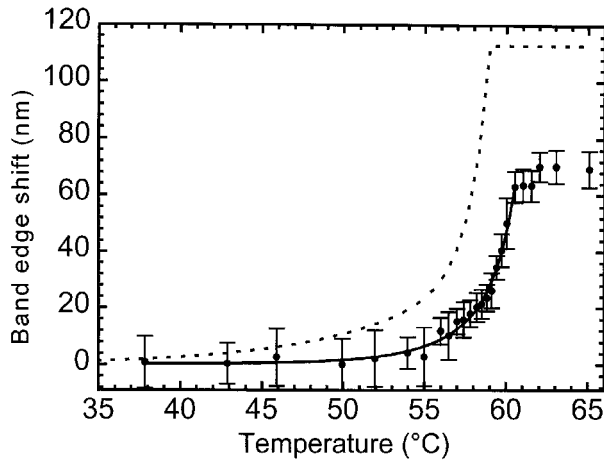


Figure 15. Temperature dependence of the bandedge shift caused by the temperature-induced phase transition of the infiltrated liquid crystal. Solid curve, fit to experimental data points; dashed curve, calculation assuming a simple axial alignment of the liquid crystal in the pores.

As proof of the latter we infiltrated a liquid crystal (E7 from EM Industries Inc.) into a two-dimensional triangular pore array with a pitch of $1.58\ \mu\text{m}$ and observed the shift of a bandedge depending on the temperature. The liquid crystal E7 is in its nematic phase at room temperature but becomes isotropic at $T > 59^\circ\text{C}$. The refractive index for light polarized along the director axis is $n_e = 1.69$ while it is only $n_o = 1.49$ for perpendicular polarization exhibiting strong anisotropy.

The transmission of H-polarized light was measured along the Γ -K direction through a $200\ \mu\text{m}$ -thick bar of the infiltrated photonic crystal. Figure 14 shows the transmission spectra obtained. At room temperature the first stopband of the H-polarization is observable in the range between 4.4 and $6\ \mu\text{m}$. Although a large bandgap for the H-polarization still exists, the complete bandgap, which is characteristic of the unfilled structure, is lost due to the lowered refractive-index contrast within the infiltrated crystal. Therefore the investigations were only carried out for H-polarization. When the structure is

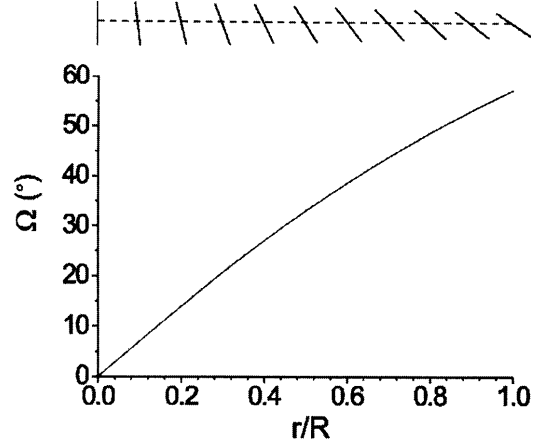


Figure 16. Alignment of the liquid crystal within a cylindrical pore in the case of ER configuration with a weak molecular anchoring strength of $W_\Theta = 1 \times 10^{-5}\ \text{J m}^{-2}$. Bottom, radial dependence of the director angle Ω . Top, orientation of the director at discrete radial positions.

heated up, the upper band edge at $4.4\ \mu\text{m}$ is red shifted while the lower bandedge exhibits no noticeable shift. At a temperature of 62°C the red shift saturates and the total shift amounts to $\Delta\lambda = 70\ \text{nm}$ as shown in figure 15. This corresponds to 3% of the bandgap width. The shift is caused by the change in orientation of the liquid-crystal molecules inside the pores. In a simplified model one can assume that all the liquid-crystal molecule directors line up parallel to the pore axis when the liquid crystal is in its nematic phase at room temperature. Then the H-polarized light sees the lower refractive index n_o inside the pores. If the temperature is increased above 59°C a phase transition occurs and the liquid-crystal molecule directors are randomly oriented. The H-polarized light now reaches a refractive index inside the pores which is an average over all these orientations. According to this model a red shift of $\Delta\lambda = 113\ \text{nm}$ is expected which is considerable larger than that measured. However, the assumption of perfect axial alignment of all the directors is questionable. From free energy considerations the escaped-radial (ER) alignment (figure 16) is expected to be the thermodynamical stable configuration of the liquid-crystal molecules within the pores. In this case only the directors in the centre of the pore are axially aligned. The directors near the pore walls are inclined. The refractive-index change from this configuration to the isotropic phase is smaller and explains the smaller bandedge shift. Moreover, the lightfields of the modes at the higher bandedge ($\lambda = 4.4\ \mu\text{m}$) are concentrated in the centre of the pores. They experience a strong refractive-index change caused by the phase transition as the initially axially-aligned directors in the pore centre switch to total random orientations. The field distribution of the modes at the lower bandedge are mainly concentrated in the silicon walls and, therefore, do not experience such a change in the refractive index so that the lower bandedge does not shift. Although the shifting or switching of a bandgap via temperature is not very practical, the present study confirms the possible tunability of photonic bandgaps using liquid crystals.

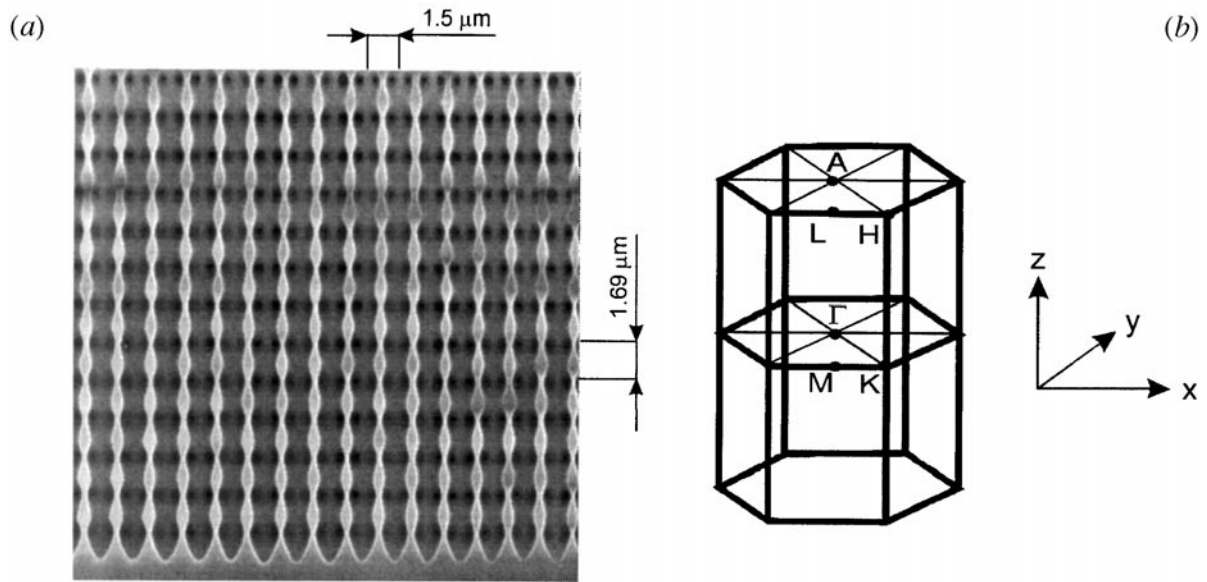


Figure 17. (a) SEM image showing a longitudinal section of the modulated pore structure. The variation in the pore diameter with depth can be modelled by a sinusoidal modulation $r = r_0 + \Delta r \sin(2\pi z/l_z)$ with $r_0 = 0.63 \mu\text{m}$, $\Delta r = 0.08 \mu\text{m}$ and $l_z = 1.69 \mu\text{m}$. (b) Hexagonal Brillouin zone showing the high-symmetry directions.

5. Three-dimensional photonic crystals based on macroporous silicon

Thus far, the main work based on macroporous silicon and photonic crystals concerned two-dimensional photonic crystals. Recently, however, attempts have been undertaken to use macroporous silicon for three-dimensional photonic crystals.

One approach for introducing a refractive-index variation in the third dimension is the modulation of the pore diameter with pore depth [25]. As described in the first paragraph of this review, the pore diameter of the macropores can be controlled during the fabrication process (photo-electrochemical etch process) by the intensity of the back illumination of the wafer. Strong illumination leads to high-etching currents and, therefore, wide pores while the opposite is valid for low illumination.

We now varied the illumination intensity periodically during the etch process applying a zig-zag profile. Figure 17(a) shows a SEM image of a longitudinal section of the sample. The pore diameter modulation can be well approximated by a sinusoidal dependence on the pore depth. The modulation period amounts to $1.69 \mu\text{m}$ and the porosity varies between 81 and 49% between the planes of wide- and narrow-pore diameters. The lattice constant a of the two-dimensional pore pattern is again $1.5 \mu\text{m}$. The resulting three-dimensional photonic crystal has a hexagonal lattice and the corresponding Brillouin zone is also hexagonal (figure 17(b)). Note, that this is the first three-dimensional photonic crystal in the IR region which perfectly extends over more than 10 lattice periods. To investigate the optical properties of the structure introduced by the pore diameter modulation we performed transmission measurements along the pore axis which correspond to the Γ -A direction. The spectrum is shown in figure 18 and compared to a three-dimensional bandstructure calculation using the plane-wave method. For comparison with the experiment, the left

side of the bandstructure shows the relevant dispersion relation along Γ -A. The stopgap in this direction caused by the periodic pore diameter modulation is indicated by a grey bar. This coincides well with the range of zero transmission between $1350 (\lambda = 7.41 \mu\text{m})$ and $1680 \text{ cm}^{-1} (\lambda = 5.95 \mu\text{m})$ measured along the pores. Although the structure does not show a complete three-dimensional bandgap it has another distinct property: as it is not based on building blocks of a fixed shape (e.g. spheres or ellipsoids) the periodicity can be different for all directions. The modulation period along the pore axis (z -axis) can be independently controlled from the periodicity in the x - y -plane. Consequently, the dispersion relation along the pores can be adjusted nearly independently from the dispersion relation perpendicular to them.

Another approach to fabricating three-dimensional photonic crystals on the basis of macroporous silicon includes a two-step process [26]. In the first step a conventional two-dimensional array of straight pores is photo-electrochemically etched. Afterwards additional pores are drilled under oblique angles from the top using a focused ion beam (FIB). In this way a set of three different pore directions is established which cross each other depthwise. The fabricated structure is very similar to the well known Yablonovite structure for the microwave region. However, a complete three-dimensional bandgap is not yet shown since the angles between the three different pore sets have not been properly aligned. Although the depth of the structure is limited due to the FIB process, this method has the potential for the fabrication of a three-dimensional photonic crystal with a complete three-dimensional bandgap.

Another fabrication technique which should give a very similar result uses the photo-electrochemical etching of macropores on a (111)Si surface [27]. In contrast to the pore growth on a (100)Si surface in the case of a (111)Si surface the pores grow into $\langle 113 \rangle$ directions. As there are three equivalent $\langle 113 \rangle$ directions available from the (111) surface, three pores start to grow from each nucleation point

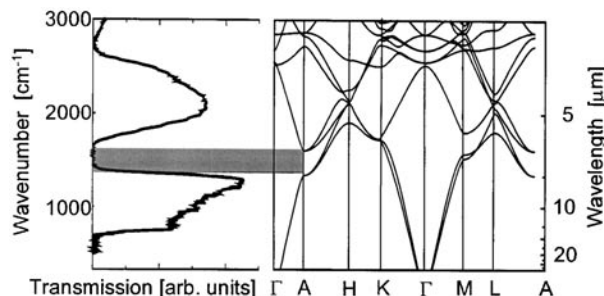


Figure 18. Transmission measured in the Γ -A direction (along the pore axis) and comparison with the calculated three-dimensional bandstructure. The grey bar indicates the stopgap for light propagation in this direction causing zero transmission.

at the surface. Bandstructure calculations for a corresponding structure show that the pores along the three $\langle 113 \rangle$ directions grow at suitable angles such that the structure should exhibit a three-dimensional complete photonic bandgap. Figure 19 shows an image of such a structure where the nucleation spots of the pores at the (111) surface are still randomly distributed. Therefore, this structure does not yet have the described long-range periodicity of crossing pores and exhibits no photonic bandgap. However, the crossing pores are clearly visible and the intended structure can be imagined.

6. Summary

In summary we have shown that macroporous silicon is a suitable material to fabricate ideal two-dimensional photonic crystals for the IR region. Due to the high-refractive-index contrast between silicon and air the bandgaps are large and for a triangular array of pores a complete bandgap for the light propagating in the plane of periodicity appears. Experimental investigations of such a structure for different porosities (r/a -values) confirms the calculated gap map and the maximum width of the complete bandgap of 16% for $r/a = 0.475$. The wide bandgap of the H-polarization causes a strong attenuation for light with frequencies within the gap. The corresponding field is exponentially damped and a damping constant of 10 dB per pore row could be experimentally determined. In addition to the bandgaps the long wavelength regime below the first bandgap was also investigated. Large birefringence was experimentally and theoretically studied and a maximum value of $\Delta n_{\text{eff}} = 0.366$ (difference between H- and E-polarization) was obtained which is by a factor of 43 larger than the birefringence of quartz. Due to the photolithographic prestructuring of the macroporous silicon, defects could intentionally be introduced. The transmission through a straight waveguide was investigated. After comparison of the experimental features with bandstructure calculations a single mode transmission in a spectral range with a bandwidth of 10% could be identified. Additionally, transmission measurements at a point defect have been performed. Two resonances with Q -values of 647 and 191 were found and comparison with theory reveals that they can be attributed to the monopole and decapole mode of the microresonator. To obtain bandgaps in the technologically interesting near-IR spectral region macroporous silicon two-dimensional photonic crystals with structure sizes of $a = 0.5 \mu\text{m}$ were fabricated. They exhibit

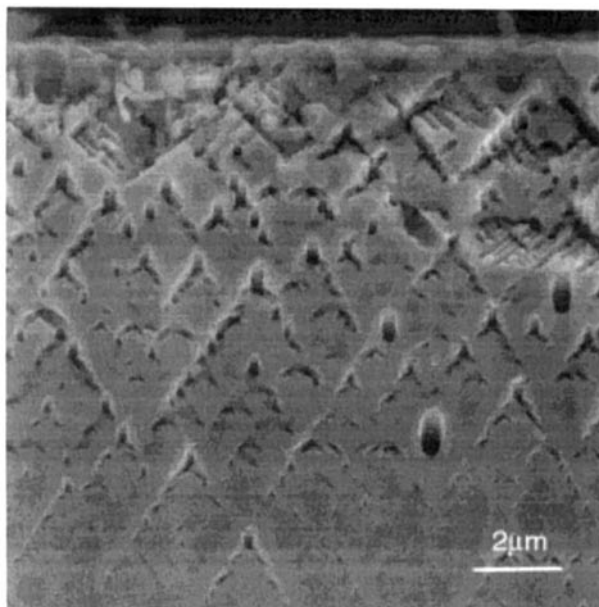


Figure 19. Crossing pores caused by the photo-electrochemical etching of a (111) n-type silicon surface. The nucleation spots of the pores at the (111) surface are random so that a strict periodic arrangement cannot yet be obtained.

bandgaps in the optical telecommunication window around $\lambda = 1.3 \mu\text{m}$ which was confirmed by reflection measurements.

Another issue, closely related to applications, is the tunability of photonic bandgaps. We demonstrated a red shift of an upper bandedge by 70 nm based on the refractive-index change due to the reorientation of liquid crystals infiltrated into the pores. The reorientation was initiated by the temperature change and corresponds to the phase transition of nematic \rightarrow isotropic of the liquid crystal.

Finally, perfect extended three-dimensional photonic crystals based on macroporous silicon were presented. Transmission measurements on these three-dimensional photonic crystals with modulated pores showed good agreement with the full three-dimensional bandstructure calculations. Although these photonic crystals do not exhibit a complete three-dimensional bandgap the dispersion relation along the pores can almost independently be tuned compared to the dispersion relation perpendicular to it. In particular, one can imagine utilizing the mode structure of these photonic crystals to realize novel atom traps [28].

All these experiments show that macroporous silicon is an ideal material to study the properties of photonic crystals in the IR regime as well as for possible technological applications operating in this spectral range.

Acknowledgments

The authors gratefully acknowledge H Föll for helpful discussions and especially appreciate the fruitful cooperation with V Lehmann, P Villeneuve, M Agio, C Soukoulis and S John.

References

- [1] Joannopoulos J D, Meade R D and Winn J N 1995 *Photonic Crystals* (Princeton, NJ: Princeton University Press)
- [2] Johnson S G, Fan S, Villeneuve P R, Joannopoulos J D and Kolodziejski L A 1999 *Phys. Rev. B* **60** 5751
- [3] Labilloy D, Benisty H, Weisbuch C, Krauss T F, De La Rue R M, Bardinal V, Houdré R, Oesterle U, Cassagne D and Jouanin C 1997 *Phys. Rev. Lett.* **79** 4147
- [4] Grüning U, Lehmann V and Engelhardt C M 1995 *Appl. Phys. Lett.* **66** 3254
- [5] Grüning U, Lehmann V, Ottow S and Busch K 1996 *Appl. Phys. Lett.* **68** 747
- [6] Lau H W, Parker G J, Greef R and Hölling M 1995 *Appl. Phys. Lett.* **67** 1877
- [7] Lehmann V and Föll H 1990 *J. Electrochem. Soc.* **137** 653
- [8] Lehmann V 1993 *J. Electrochem. Soc.* **140** 2836
- [9] Meade R D, Brommer K D, Rappe A M and Joannopoulos J D 1992 *Appl. Phys. Lett.* **61** 495
- [10] Sakoda K 1995 *Phys. Rev. B* **52** 8992
- [11] Robertson W M, Arjavalingam G, Meade R D, Brommer K D, Rappe A M and Joannopoulos J D 1992 *Appl. Phys. Lett.* **61** 495
- [12] Sakoda K 1995 *Phys. Rev. B* **52** 7982
- [13] Leonard S W, van Driel H M, Busch K, John S, Birner A, Li A-P, Müller F, Gösele U and Lehmann V 1999 *Appl. Phys. Lett.* **75** 3063
- [14] Kirchner A, Busch K and Soukoulis C M 1998 *Phys. Rev. B* **57** 277
- [15] Halevi P, Krokhin A A and Arriaga J 1999 *Appl. Phys. Lett.* **75** 2725
- [16] Genereux F, Leonard S W, van Driel H M, Birner A and Gösele U 2001 *Phys. Rev. B* **63** 161101(R)
- [17] Netti M C, Harris A, Baumberg J J, Whittaker D M, Charlton M B D, Zoorob M E and Parker G J 2001 *Phys. Rev. Lett.* **86** 1526
- [18] Leonard S W, van Driel H M, Birner A, Gösele U and Villeneuve P R 2000 *Opt. Lett.* **25** 1550
- [19] Benisty H, Olivier S, Rattier M and Weisbuch C 2001 *Photonic Crystals and Light Localization in the 21st Century* (New York: Kluwer Academic) pp 117–28
- [20] Kramper P, Birner A, Agio M, Soukoulis C, Gösele U, Mlynek J and Sandoghdar V *Phys. Rev. B* to be published
- [21] Bell P M, Pendry J B, Martin Moreno L and Ward A J 1995 *Comput. Phys. Commun.* **85** 306
- [22] Rowson S, Chelnokov A, Cuisin C and Lourtioz J-M 1999 *J. Opt. A: Pure Appl. Opt.* **1** 483
- [23] Rowson S, Chelnokov A and Lourtioz J-M 1999 *Electron. Lett.* **35** 753
- [24] Busch K and John S 1999 *Phys. Rev. Lett.* **83** 967
- [25] Schilling J, Müller F, Matthias S, Wehrspohn R B and Gösele U 2001 *Appl. Phys. Lett.* **78** 1180
- [26] Chelnokov A, Wang K, Rowson S, Garoche P and Lourtioz J-M 2000 *Appl. Phys. Lett.* **77** 2943
- [27] Christophersen M, Carstensen J, Feuerhake A and Föll H 2000 *Mater. Sci. Eng. B* **69–70** 194
- [28] Toader O, John S and Busch K 2001 *Opt. Exp.* **8** 217